Determination of J—Experimental Method for Bend Specimens (continued)

$$J = -\left(\frac{\partial PE}{\partial a}\right)_M = \int_0^M \frac{\partial \theta(\tilde{M}, a)}{\partial a} d\tilde{M} = -\int_0^M \frac{\partial \theta_{cr}(\tilde{M}, c)}{\partial c} d\tilde{M} \quad \text{because} \quad \frac{\partial(\ )}{\partial a} = -\frac{\partial(\ )}{\partial c}$$

Now note: $\left(\frac{\partial \theta_{\text{cr}}}{\partial \text{c}}\right)_M = -2\frac{\partial f}{\partial \mu}\frac{M}{\sigma_Y c^3}$, with $\mu = \frac{M}{\sigma_Y c^2}$, and $\left(\frac{\partial \theta_{\text{cr}}}{\partial M}\right)_c = \frac{\partial f}{\partial \mu}\frac{1}{\sigma_Y c^2}$

Thus, $\left(\frac{\partial \theta_{\text{cr}}}{\partial \text{c}}\right)_M = -\left(\frac{\partial \theta_{\text{cr}}}{\partial M}\right)_c \frac{2M}{c}$, and

$$J = \frac{2}{c}\int_0^M M d\theta_{cr}$$

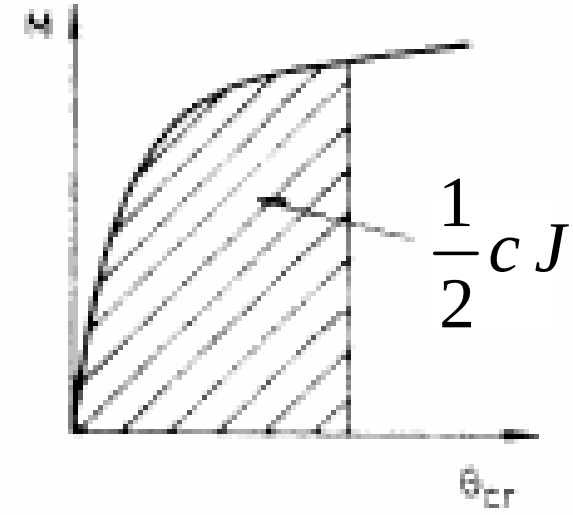

Conclusion: For the deeply cracked bend specimen J can be determined directly as the area under the moment-rotation (cr) curve.

J-Resistant Curve Data for a Tough Pressure Vessel Steel—A533B

Determined using compact tension specimens under large scale yielding

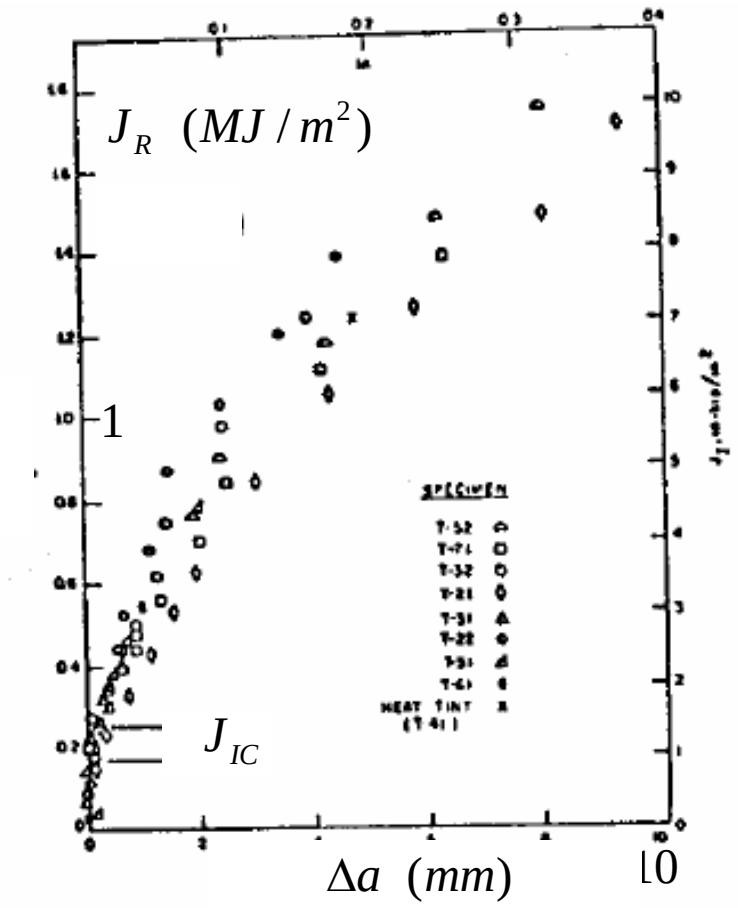

Fig. (13.3). J-resistance curves for A533B material 2 tested, at 93°C - 4T side-grooved compact specimens.

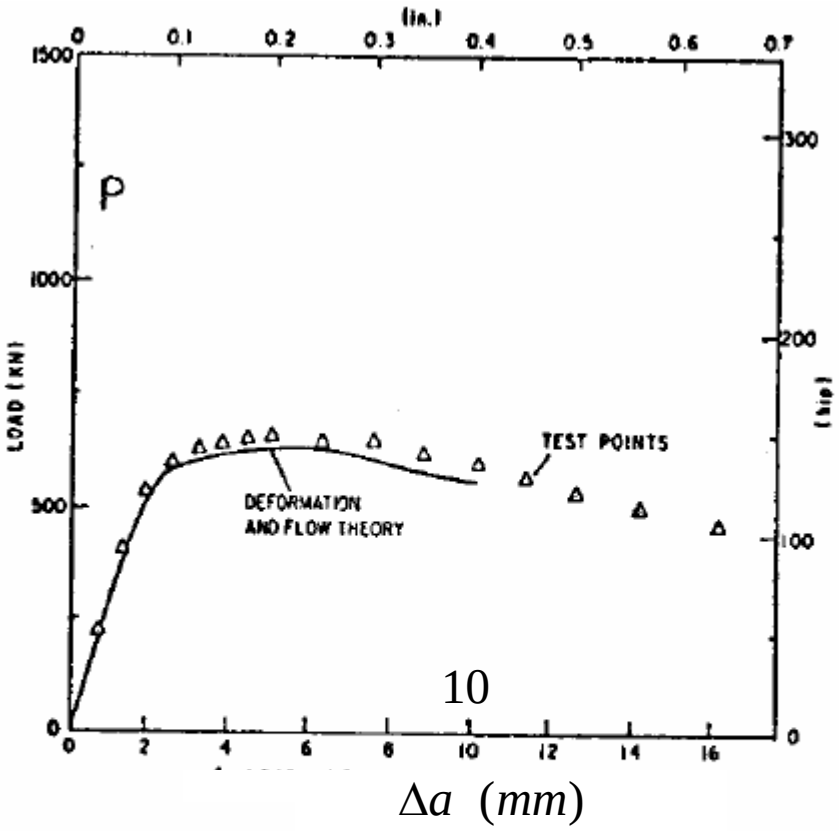

Fig. (13.5). Applied load vs. load-line displacement for 4T compact specimen T52, 25% side-grooved, $(W - a_o)$ = 86 mm (3.385 in.).

Limitations of Large Scale Yielding Crack Analysis Pg 70 of notes

The HRR fields suggest that there will be a J-dominated crack tip field in a hardening material. In principle that is the case at sufficiently low J, but in practice the level of J to which J-dominance holds depends strongly on the geometry of the body. Consider The following three geometries. The two on the left provide the necessary constraint Such that the high stress triaxiality associated with the plane strain J-fields is preserved Deep into the plastic range. The configuration on the right allows the stress ahead of The tip to be relaxed as the plastic zone begins to "feel" the boundary and J-dominance is Quickly eroded.

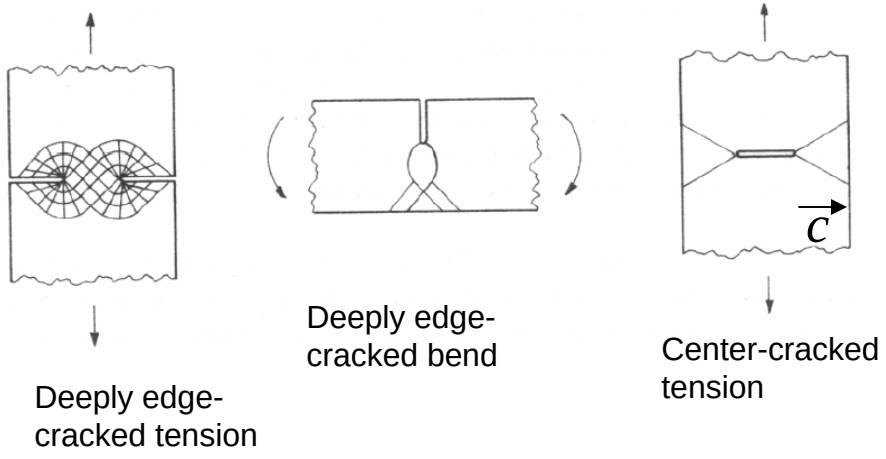

Deeply edge-cracked tension

Deeply edge-cracked bend

Center-cracked tension

Slip line fields of perfect plasticity

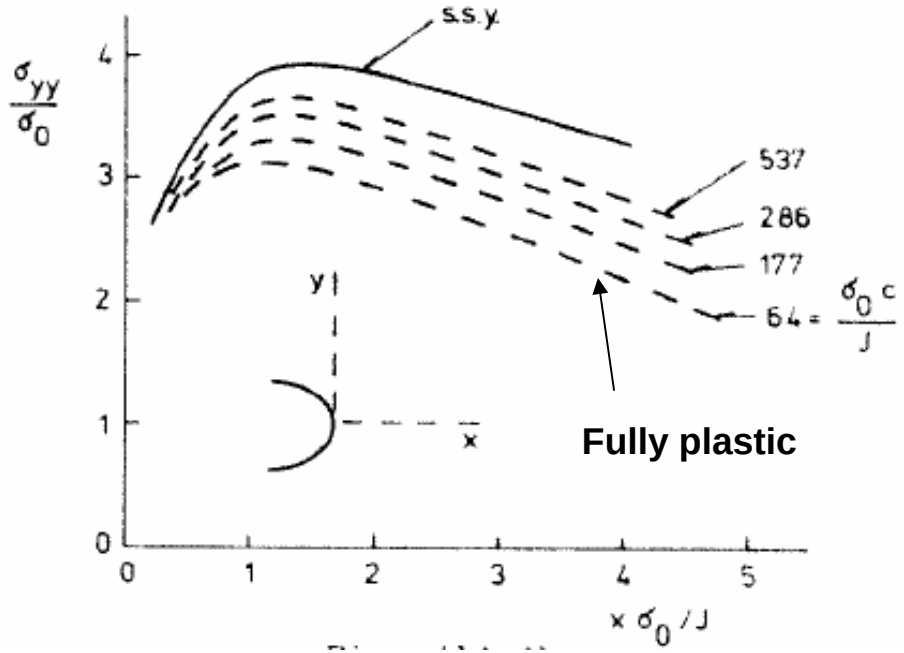

Erosion of J-dominance in center-cracked Specimen as plastic zone grows.
McMeeking and Parks (1978)

Stability of Crack Growth under Large Scale Yielding

With reference to the three-point bend geometry in series with a linear spring. As shown in Hutchinson & Paris (1978), for a deeply cracked beam (c<b/2):

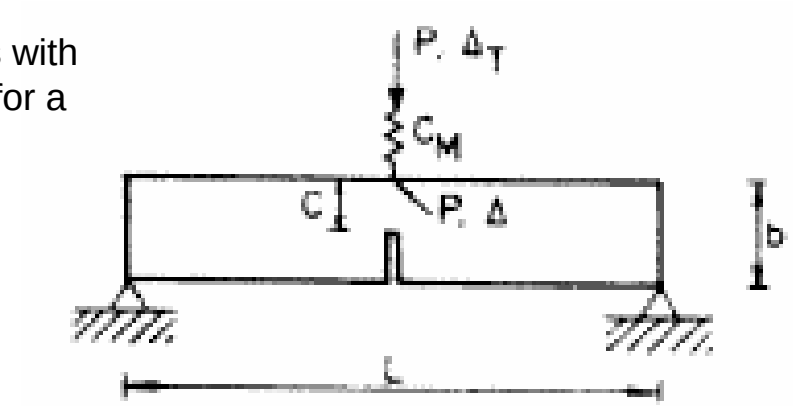

$$J = \frac{2}{c}\int_0^{\Delta_{cr}} P d\Delta_{cr} \quad \text{(prior to crack advance)}$$

$$J = 2\int_0^{\Delta_{cr}} \frac{P}{c} d\Delta_{cr} - \int_{a_0}^{a} \frac{J}{c} da \quad \text{(after onset of crack growth)}$$

$$\left(\frac{\partial J}{\partial a}\right)_{\Delta_T} = \frac{4P^2}{c^2}\frac{C_M}{1 + C_M\left(\frac{\partial P}{\partial \Delta_{cr}}\right)_a} - \frac{J}{c};$$

$$\lim_{C_M\to\infty}\left(\frac{\partial J}{\partial a}\right)_{\Delta_T} = \left(\frac{\partial J}{\partial a}\right)_P = \frac{4P^2}{c^2}\left(\frac{\partial \Delta_{cr}}{\partial P}\right)_a - \frac{J}{c}; \quad \lim_{C_M\to 0}\left(\frac{\partial J}{\partial a}\right)_{\Delta_T} = \left(\frac{\partial J}{\partial a}\right)_{\Delta} = -\frac{J}{c};$$

Stability of Crack Growth under J - dominance Conditions.

Stability requires:

$$\left(\frac{\partial J}{\partial a}\right)_{\Delta_T} < \frac{dJ_R(\Delta a)}{d\Delta a}$$

See next overhead for a test series

Stability of Crack Growth under Large Scale Yielding—continued

Experiments of Paris, et al. varying the compliance.

$$T = \frac{E}{\sigma_Y^{\,2}}\left(\frac{\partial J}{\partial a}\right)_{\Delta_T}$$

$$T_R = \frac{E}{\sigma_Y^{\,2}}\left(\frac{dJ_R}{d\Delta a}\right) = 36$$

EXPERIMENTS OF PARIS, TADA, ZAHOOR AND ERNST

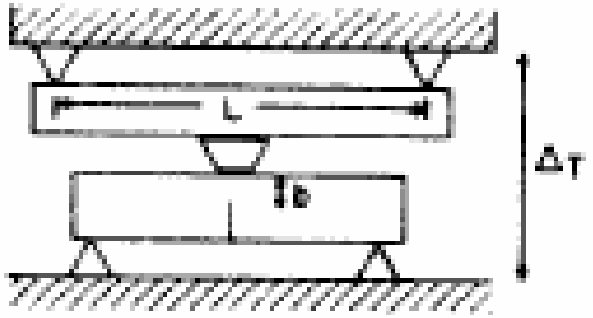

ASTM-471 ROTOR STEEL
(Ni-Cr-Mo-V)

8° ≤ Leq-valent ≤ 76°

-2 ≤ (Tapplied)at initiation ≤ 45

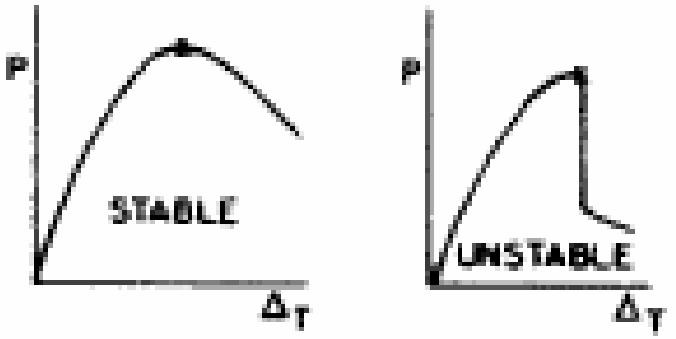

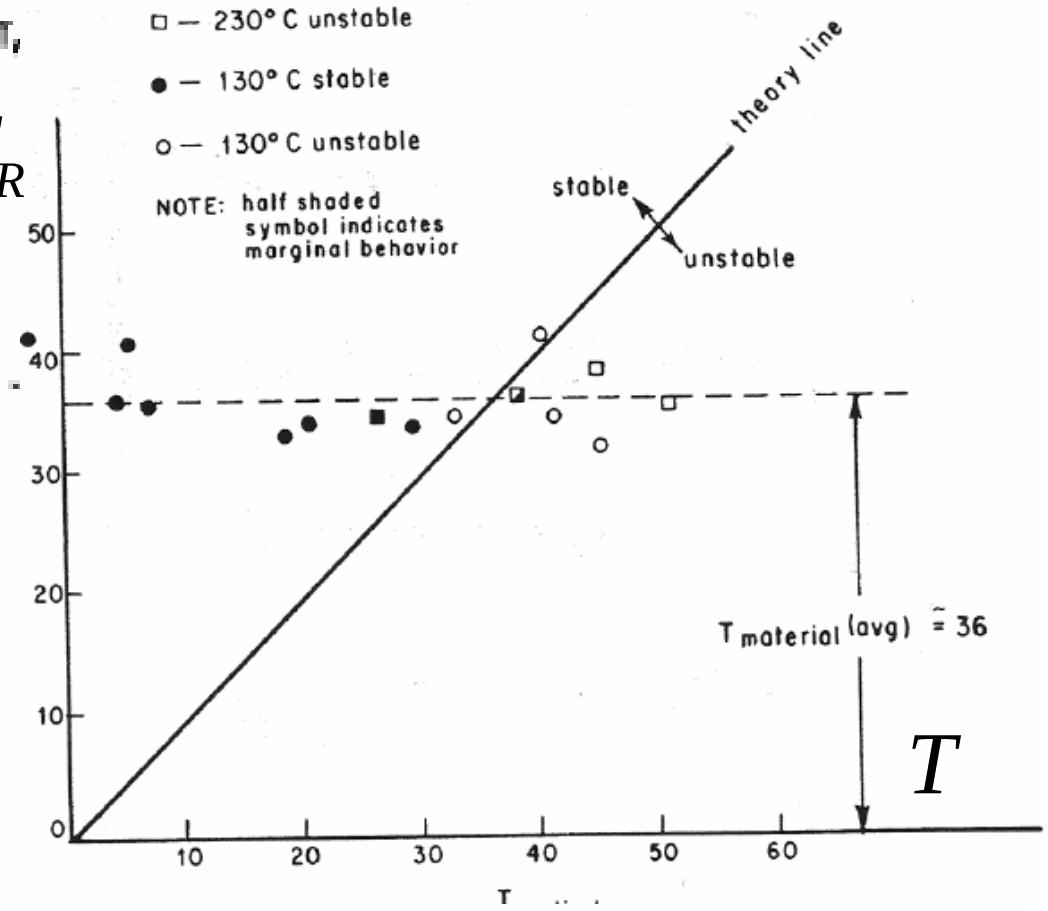

Crack Tip Opening Displacement in Plane Strain, Mode I:
Based on HRR fields (Small Strain Theory) Notes pg 78, Ref. Shih (1978)

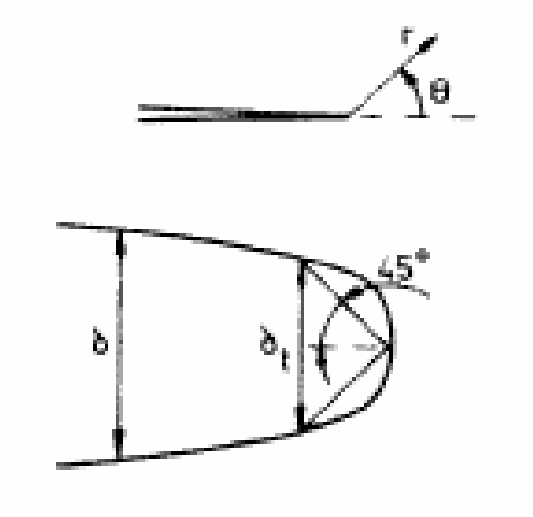

$$\delta_t = d\left(\sigma_Y / E, N\right)\frac{J}{\sigma_Y}$$

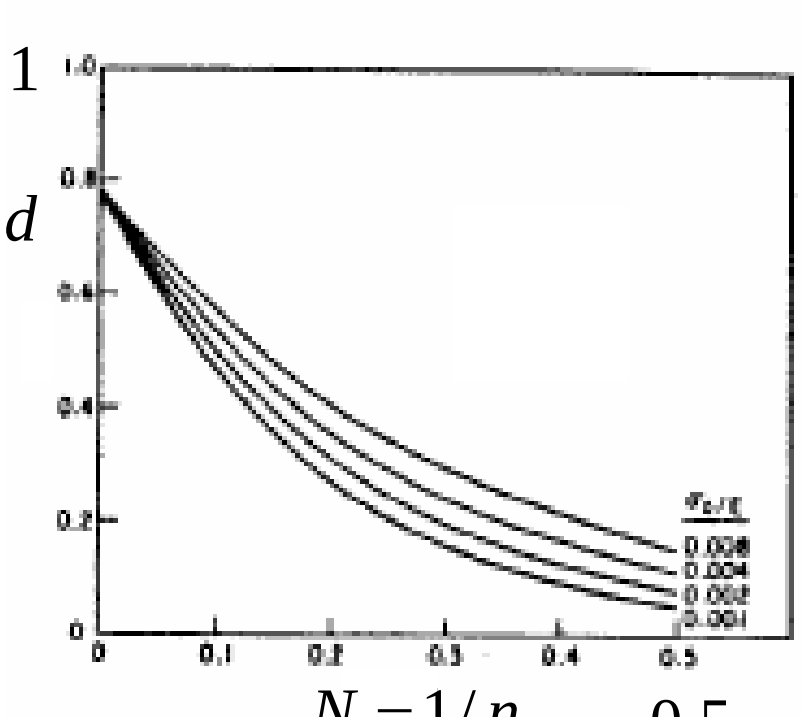

$N = 1/n$ 0.5

Power-law material

Crack Tip Opening & Stresses in Plane Strain, Mode I:
Based on Finite Strain Theory, Ref. Rice & Johnson (1970) & McMeeking (1977)

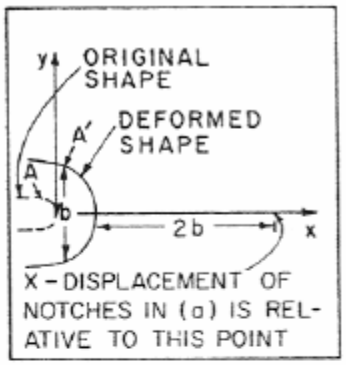

FINITE ELEMENT RESULTS

N = 0
N = 0.1
N = 0.2

$\frac{\sigma_0}{E} = \frac{1}{300}$

N = 0 $\frac{\sigma_0}{E} = \frac{1}{100}$

SLIP-LINE RESU

RICE AND

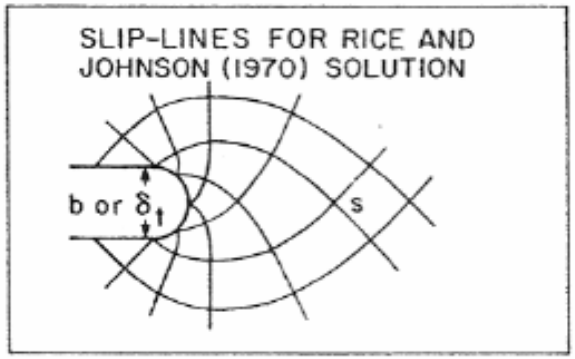

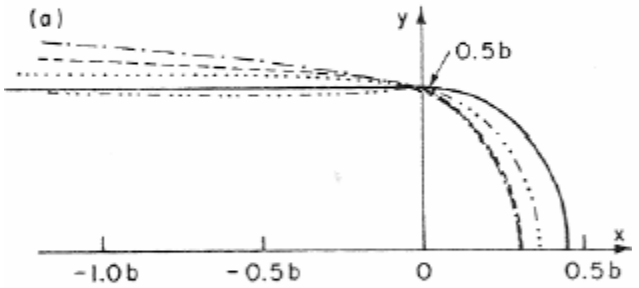

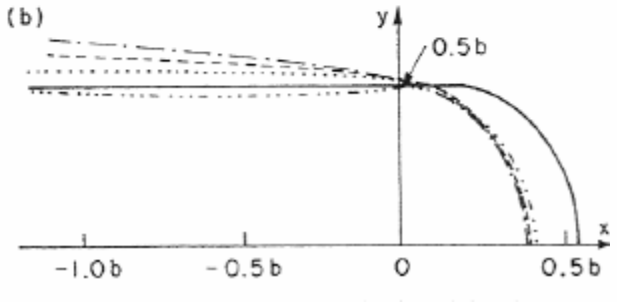

Two Fracture Mechanism in Structural Metals: Void growth & Cleavage

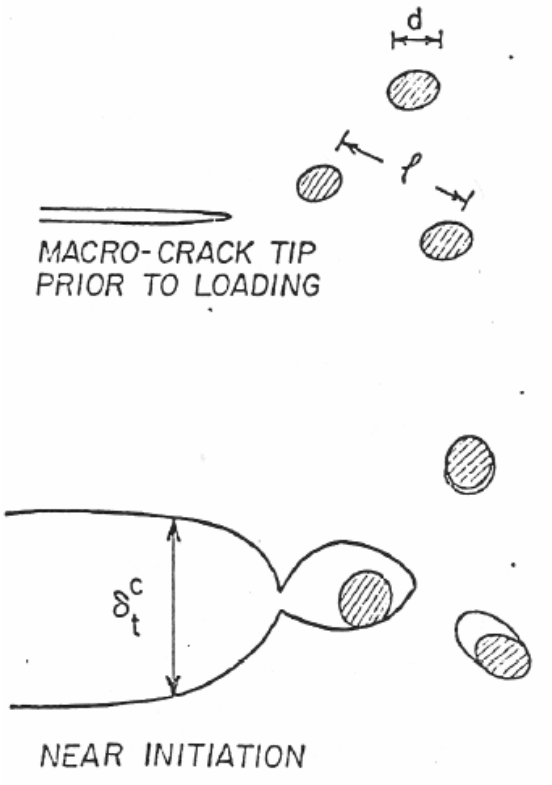

Void nucleation, growth and coalescence. Void nucleate due to debonding or cracking of second phase particles, typically micron sized.

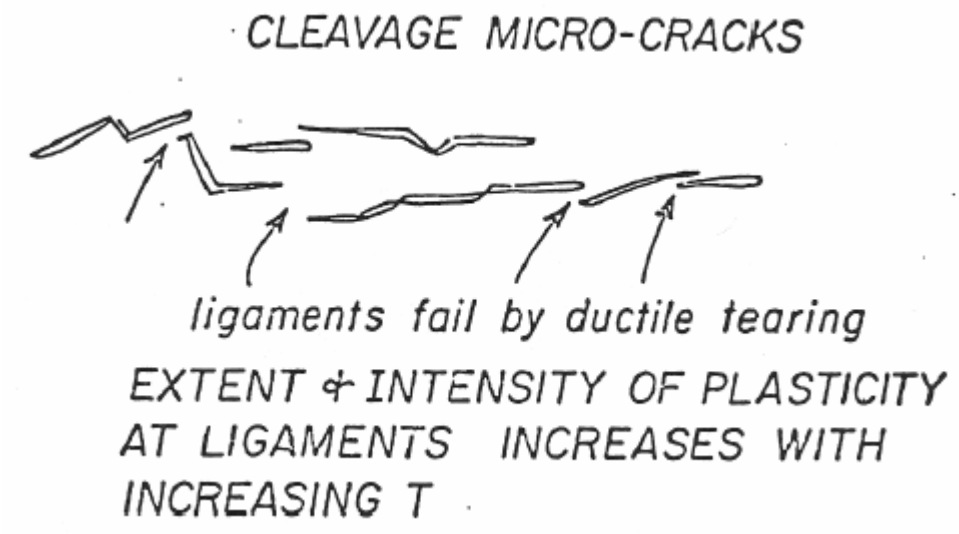

Micro-cleavage cracks occur within single crystal grains of polycrystalline material. In some cases the cracks form on grain boundaries. These cracks link up to form a macro-crack. Most dissipation of energy is due to plastic tearing of ligaments between micro cracks.

Most FCC metals (e.g., Al, Cu) do not cleave except under extraordinary circumstances.

Temperature-dependence of Fracture Toughness for A533B Steel

Ref. Parks (1976)

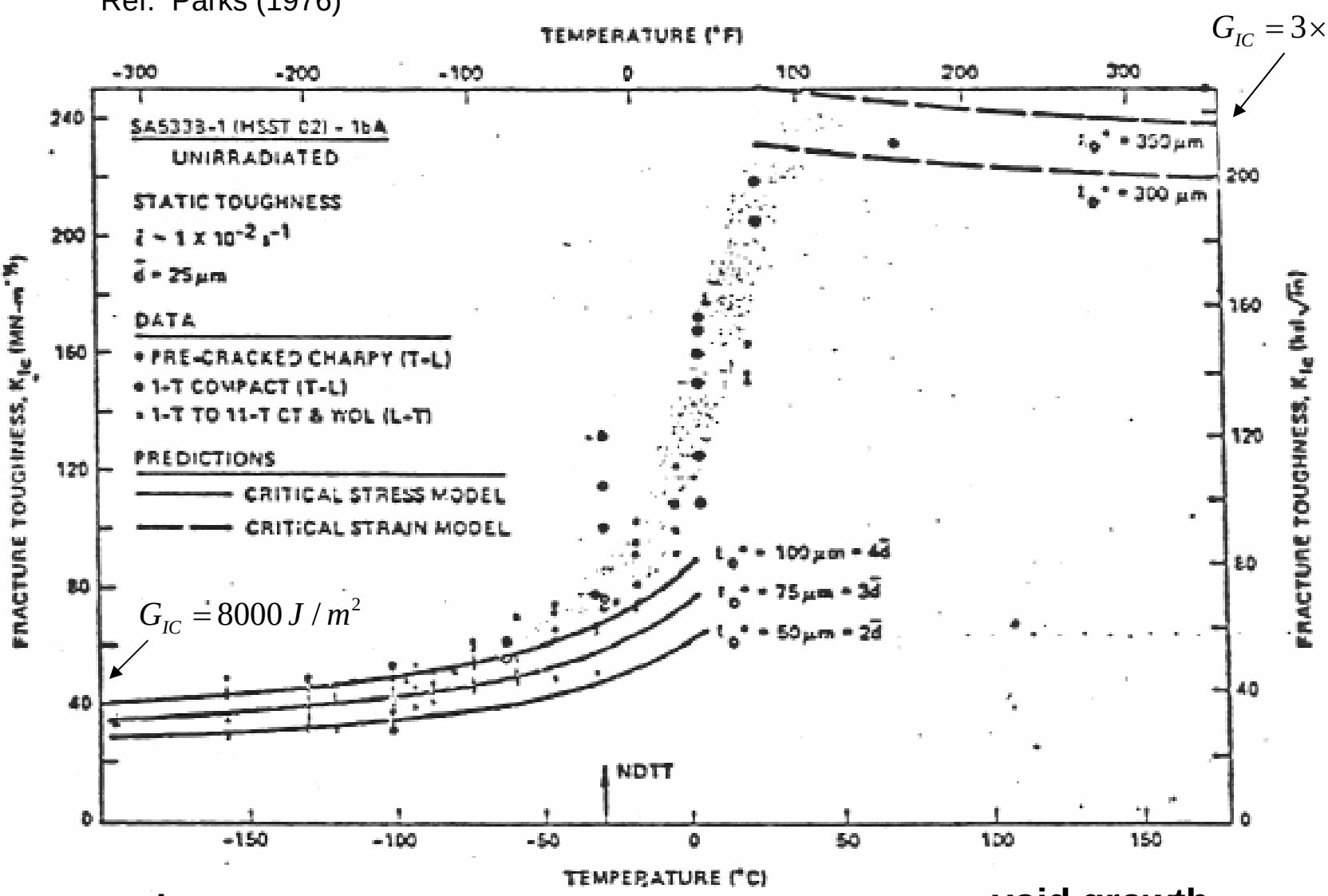

cleavage **transition** **void growth**

Ductility (tensile fracture strain) as dependent of volume fraction of second phase particles (cementite) in spheroidized steels

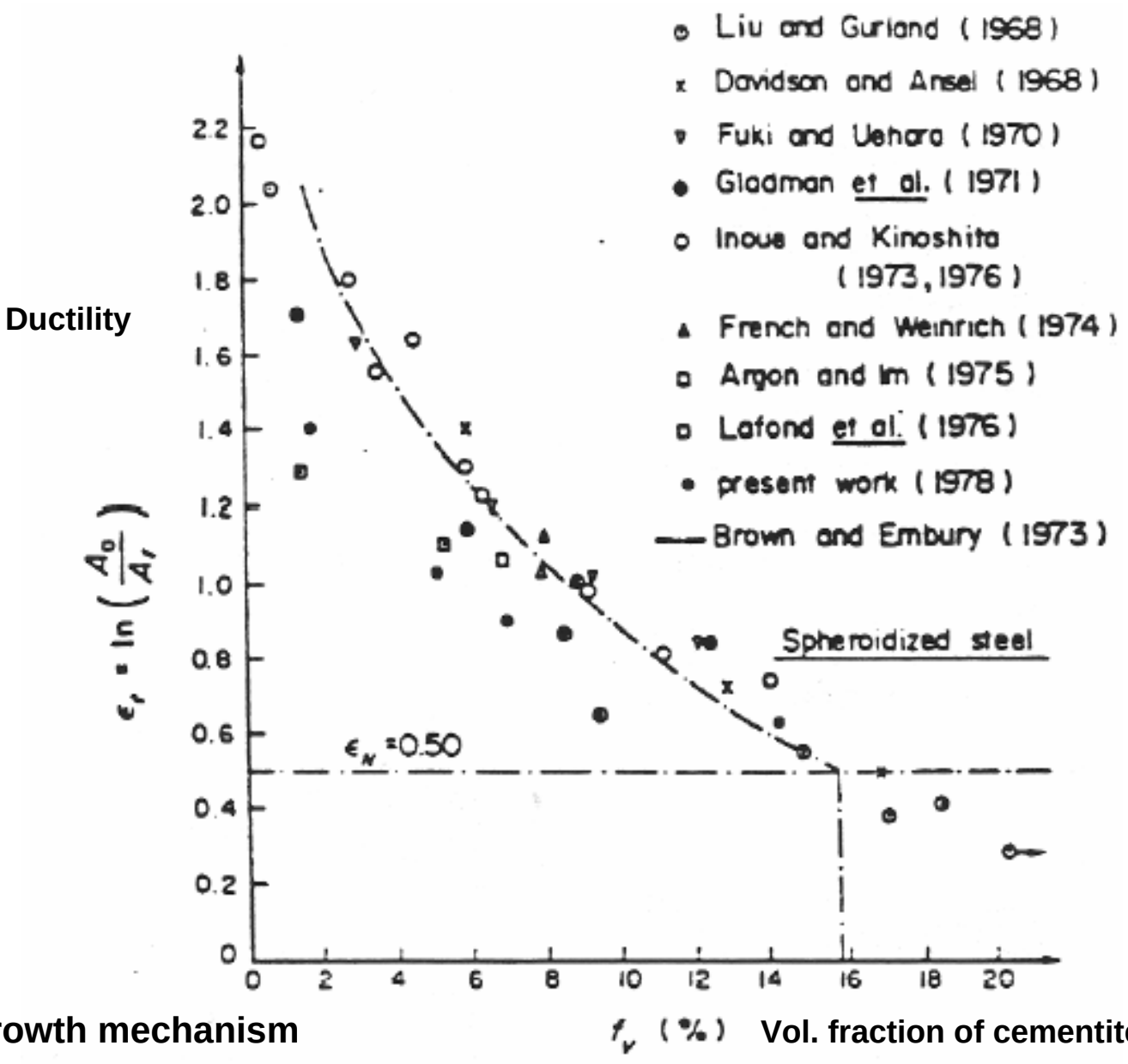

Void growth mechanism

Vol. fraction of cementite particles

FEM Simulations of Crack Growth due to Void Growth and Coalescence

Ref. Tvergaard & Hutchinson (2002)

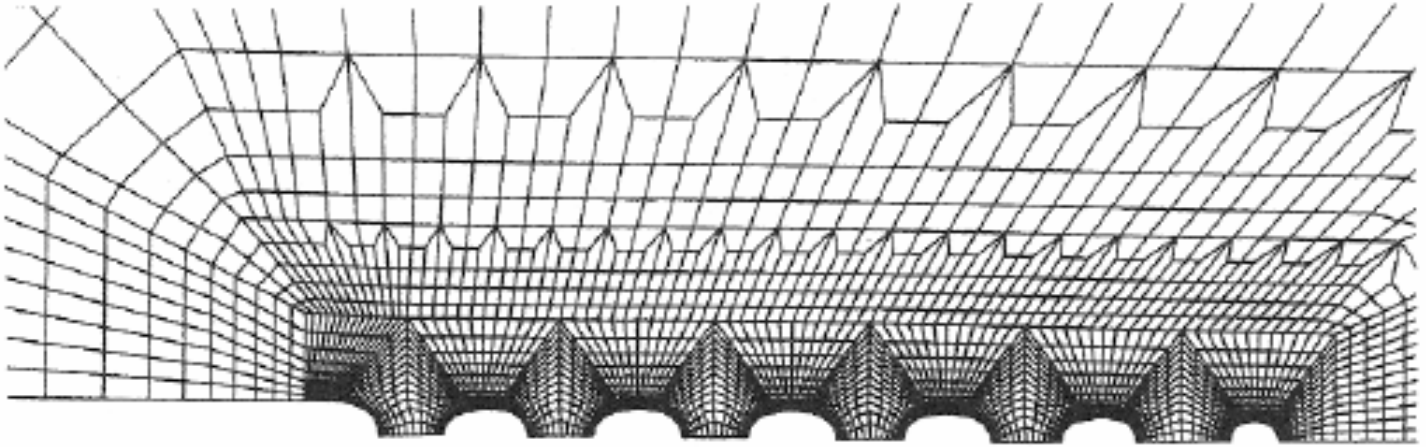

(a) Initial void vol. fraction: $f_0 = 0.014$ (Multiple void localization)

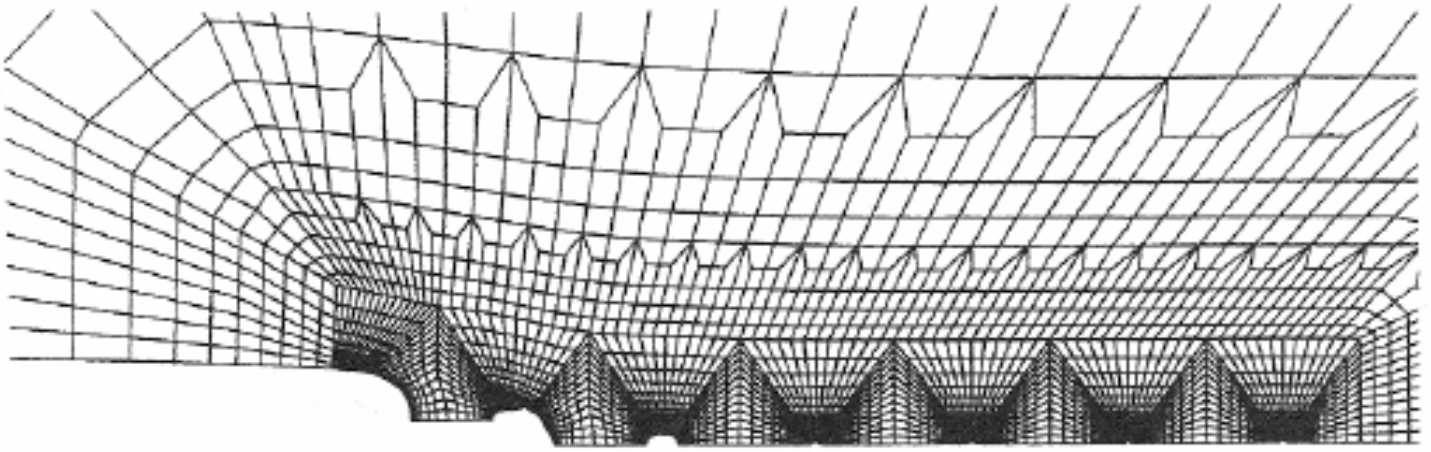

(b) Initial void vol. fraction: $f_0 = 0.00087$ (void by void growth)

Predictions of JIC Based on Void Growth Models

$$\sigma_Y = 500MPa$$

$$X_0 = 10\mu m$$

$$J_{IC} = 4\sigma_Y X_0 = 2\times10^4 J/m^2$$

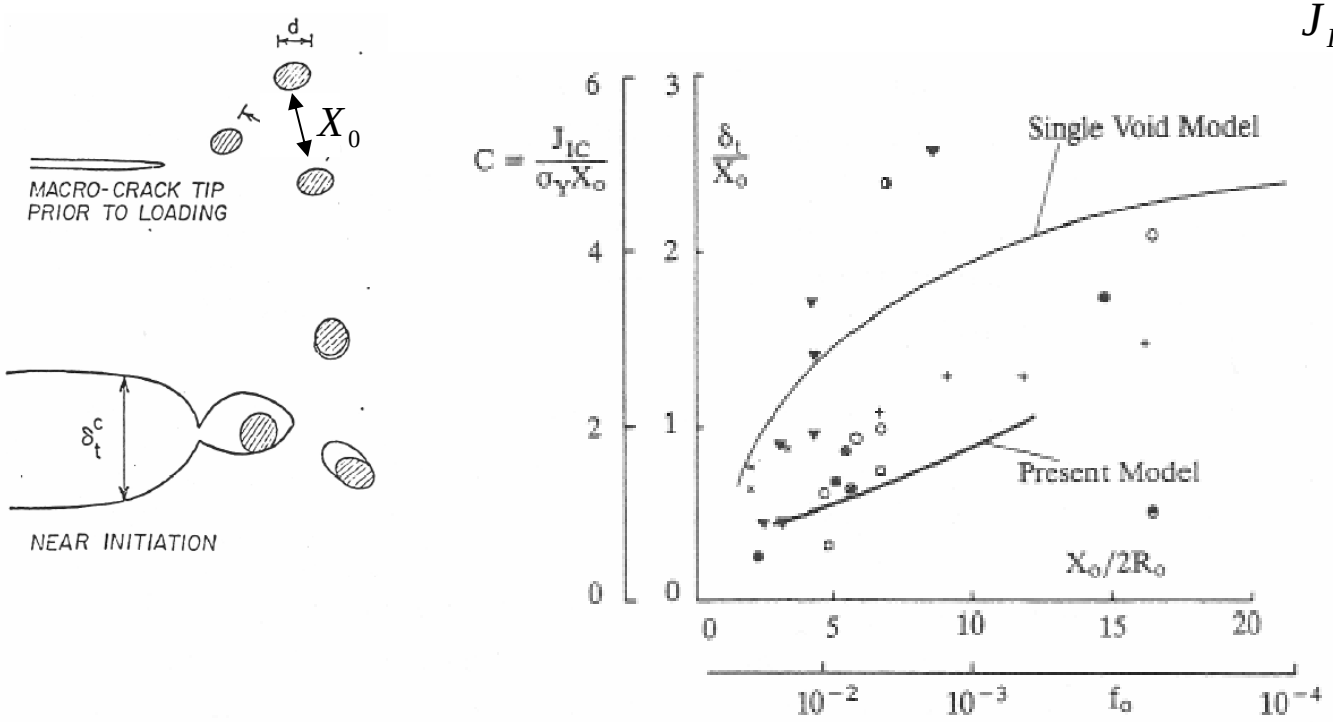

Fig. 12. Original experimental data of critical crack tip opening displacement, δ_t/X_0 versus dimensionless void nucleating particle characteristic, $X_0/(2R_0)$, assembled by McMeeking (1977), including the upper curve as the theoretical prediction for model of Rice and Johnson (1970) based on the single void mechanism. As discussed in the text, a new ordinate, $C \equiv J_{Ic}/(\sigma_Y X_0) = 2\delta_t/X_0$, and a new abscissa, $f_0 = (2R_0/X_0)^3$, have been superimposed on the figure. The prediction from the present two-dimensional discrete void model is included (the result from Fig. 2 with $\chi_c = 0.3$, $r_0/X_0 = 0.1$, $N = 0.1$, $\sigma_Y/E = 0.003$ and $\nu = 0.3$).

Modeling Traction-separation Behavior for Planar Arrays of Voids

Ref. Tvergaard & Hutchinson (2002)

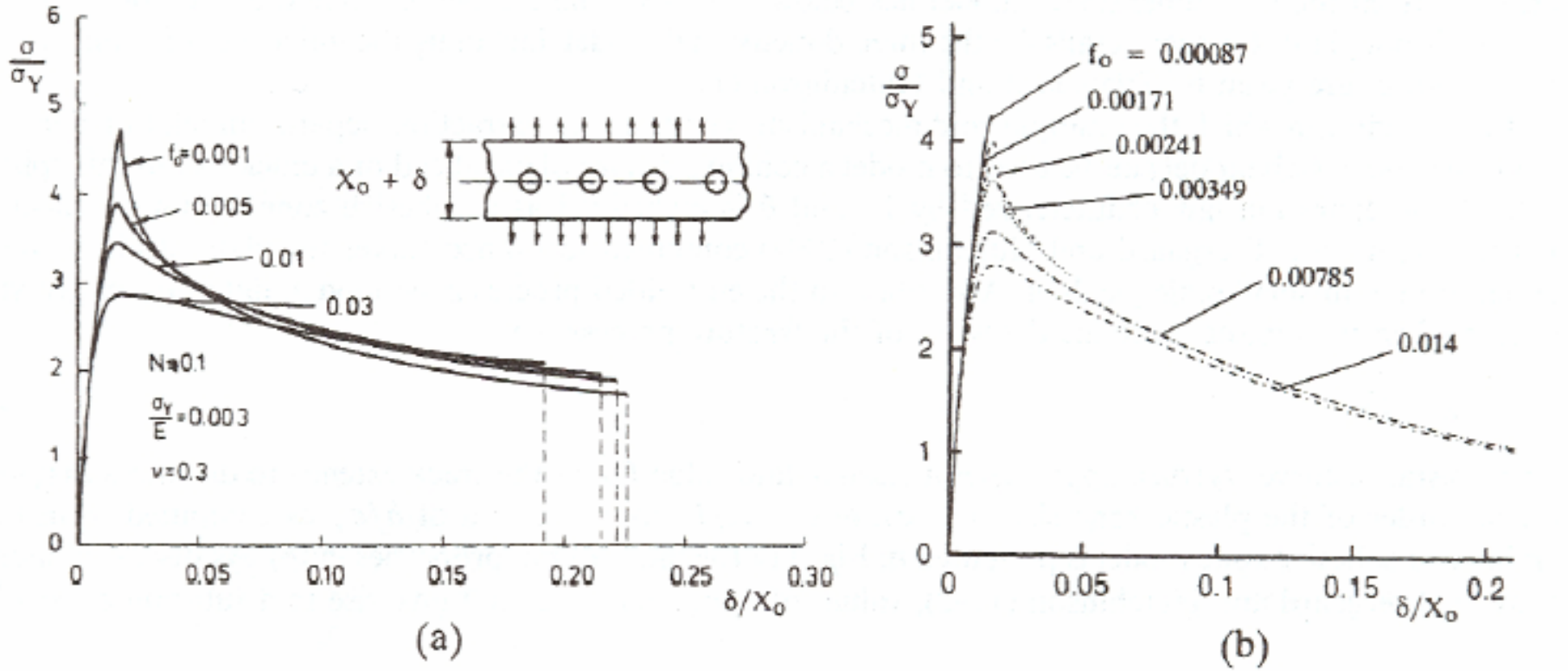

Fig. 9. Traction–separation curves for the multiple void mechanism as computed for an infinite planar slab of initial height X_0 subject to uniform normal separation of the top and bottom faces: (a) for initially spherical voids as modeled by the Gurson model under conditions of uniaxial straining (Tvergaard and Hutchinson, 1992) and (b) for two-dimensional cylindrical voids as computed using the present finite strain, plane strain formulation. Definitions of the initial void volume fractions are given in the text. For both cases, $N = 0.1$, $\sigma_Y/E = 0.003$ and $\nu = 0.3$.

Hahn, et al. (1959) Experimental Observations of Cleavage in a Large Grain Silicon Steel

grain size=100μm (0.1mm)

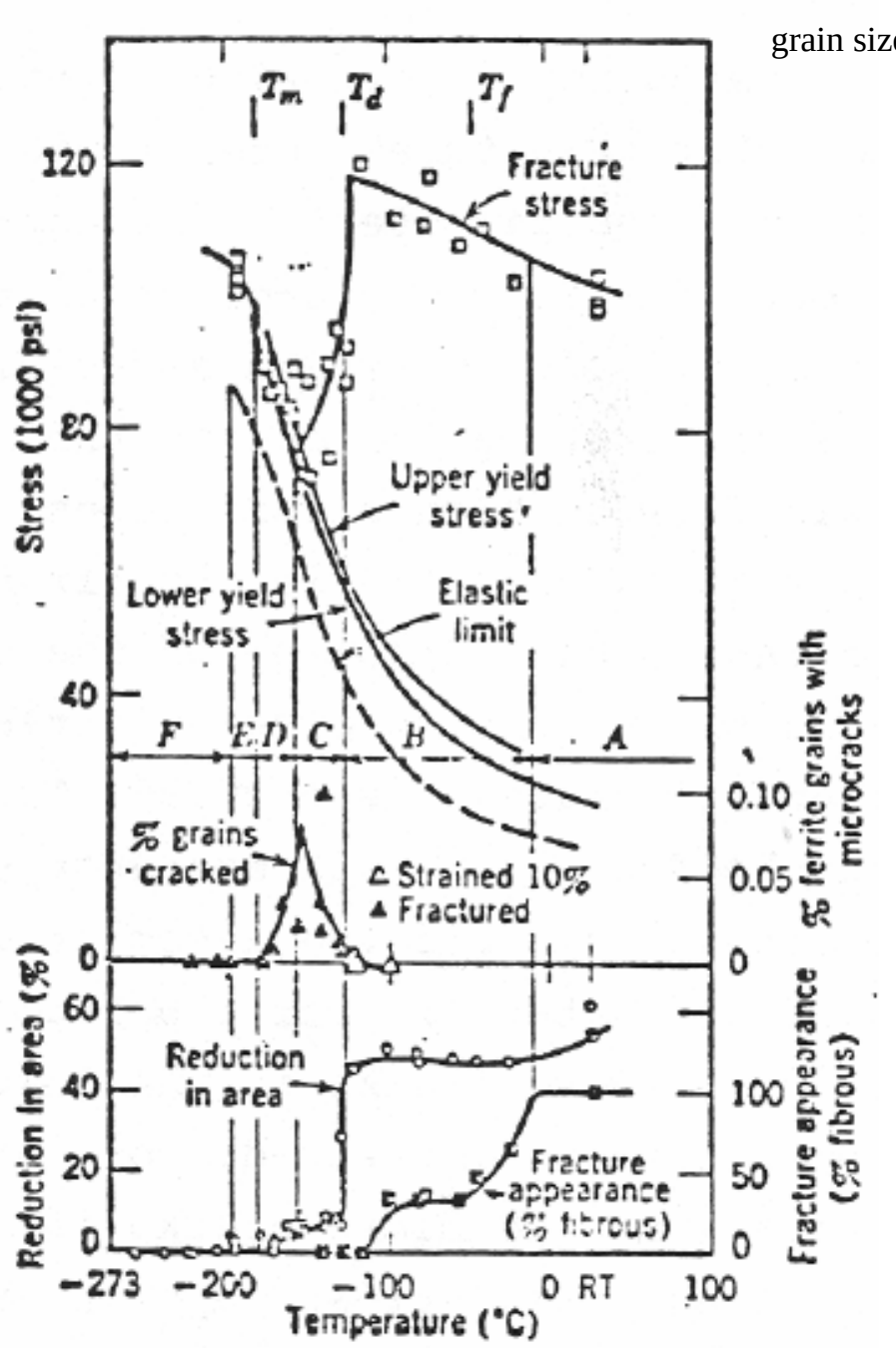

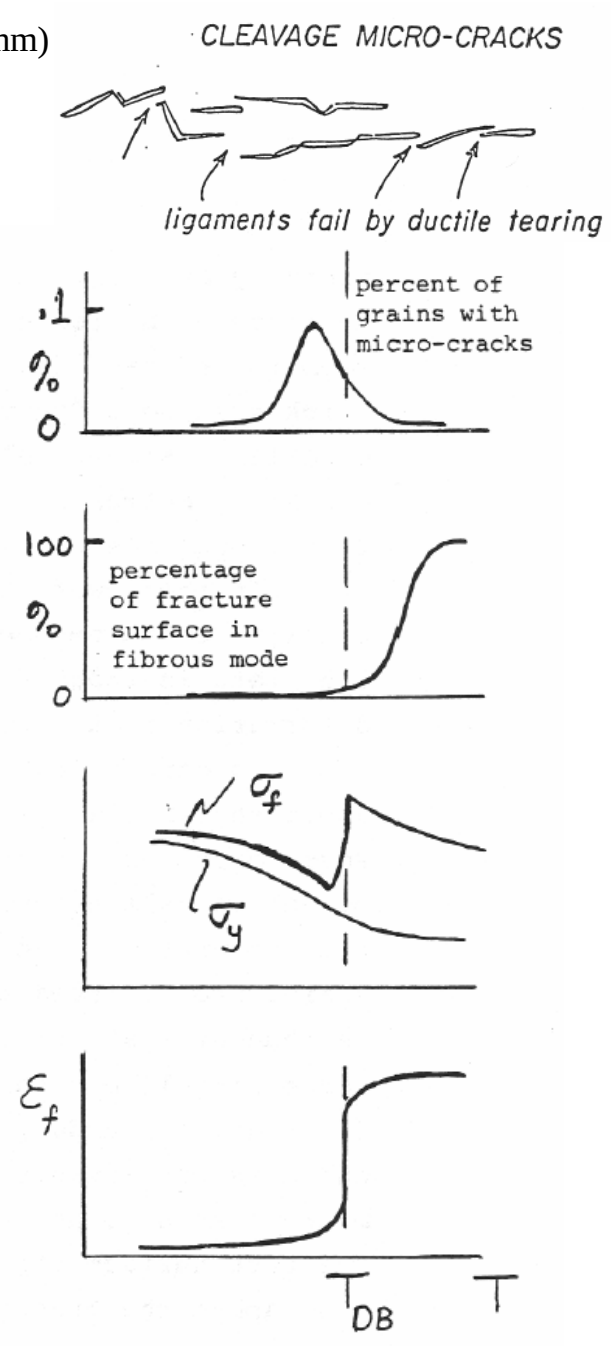

RKR Model (Ritchie, Knott & Rice, 1973) **for KIC in Cleavage Range & Predicting Transition**